INSTITUTE OF PHYSICS PUBLISHING CLASSICAL AND QUANTUM GRAVITY

Class. Quantum Grav. **23** (2006) 2665–2680 doi:10.1088/0264-9381/23/7/026

Kelvin probe measurements: investigations of the patch effect with applications to ST-7 and LISA

N A Robertson[1], J R Blackwood[2], S Buchman[1], R L Byer[1], J Camp[2], D Gill[1], J Hanson[1], S Williams[1] and P Zhou[1]

[1] Hanson Experimental Physics Laboratory, Stanford University, Stanford, CA 94305, USA
[2] NASA Goddard Space Flight Center, Greenbelt, MD 20771, USA

Received 15 November 2005, in final form 16 February 2006
Published 17 March 2006
Online at stacks.iop.org/CQG/23/2665

Abstract

One of the possible noise sources for the space-based gravitational wave detector LISA (the Laser Interferometer Space Antenna), associated with its test masses, is that due to spatial variations in surface potential (or patch effect) across the surfaces of the test mass and its housing. Such variations will lead to force gradients which may result in a significant acceleration noise term. Another noise source is that due to temporal variations in the surface potential, which in conjunction with any ambient dc voltage or net free charge on the test mass may also produce a significant acceleration noise term. The ST-7 demonstrator mission is designed to test technologies for LISA, including the gravitational reference sensor, which contains a gold-coated gold/platinum (Au/Pt) alloy test mass, surrounded by a housing that carries the electrodes for sensing and control. We have used a Kelvin probe at the Goddard Space Flight Center to make spatial and temporal measurements of contact potential differences for a selection of materials (Au/Pt, beryllia, alumina, titanium) and coatings (gold, diamond-like carbon, indium tin oxide, titanium carbide). Our investigations indicate that subject to certain assumptions all of these coatings appear to satisfy the ST-7 requirement that patch effect spatial variations should be less than 100 mV. The data also revealed evidence of behavioural trends with pressure and possible contamination effects. Regarding temporal variations, the current accuracy of the instrument is limiting the measurements at a level above the likely LISA requirements. We discuss our results and draw some conclusions of relevance to LISA.

PACS numbers: 04.80.Nn, 07.87.+v, 73.40.Cg, 95.55.Ym

(Some figures in this article are in colour only in the electronic version)

1. Introduction

LISA, the Laser Interferometer Space Antenna, [1] is a dedicated space-based gravitational wave observatory, proposed as a joint ESA/NASA mission. LISA will detect gravitational waves by measuring changes in the separation between freely-falling test masses. The effects of spatial variations in the surface potential (or patch effect) across the surface of the test mass and its housing have been identified as a possible source of noise for LISA [2, 3]. Such variations will lead to force gradients which, due to relative motion of the test mass and the surrounding spacecraft, may result in an acceleration noise term which could contribute significantly to the overall noise budget. Another noise source is that due to temporal variations in the surface potential, which in conjunction with any ambient dc voltage or net free charge on the test mass may also produce a significant acceleration noise term [3, 4].

The ST-7 demonstrator mission [5], intended to fly on ESA's LISA Pathfinder, is designed to test several of the technologies required for LISA. In particular, at the heart of ST-7 is the gravitational reference sensor, GRS, which contains a cubic test mass composed of a gold/platinum alloy coated with gold and surrounded by a housing which carries the electrodes for electrostatic sensing and control. We have carried out spatial and temporal investigations of contact potential differences on several test samples of different materials and coatings that might be used for the test mass and its housing in ST-7. This work has been done using a Kelvin probe [6] at the Goddard Space Flight Center (GSFC). We present here a summary of the results we have obtained and our analysis and conclusions to date. While this work was of immediate application to the choice of materials for ST-7, it is also very relevant to the LISA mission[3].

2. Theory

To ensure that the test masses in LISA are freely-falling in their sensitive direction and not influenced by external forces such as those due to solar radiation pressure, a drag-free system is used. Forces acting on the spacecraft result in changes in the relative position of the test mass and spacecraft. These changes are sensed and the resulting signal, suitably amplified and filtered, is applied to microthrusters to hold the spacecraft at a constant separation from the test mass, resulting in a drag-free system. However, such a feedback system will not be perfect, and in particular there will be some small residual relative motion of the test mass and spacecraft of order 1 nm $\mathrm{Hz}^{-1/2}$ over the frequencies of interest (10^{-4} to 10^{-1} Hz). Any force gradient between the test mass and the surrounding spacecraft introduces a stiffness term which in conjunction with the residual relative motion will produce an acceleration noise which could limit the sensitivity of LISA. Patch effects could produce such stiffness terms.

The patch effect refers to spatial variations in surface potential. Different metals have different work functions, where the work function, W, is the minimum energy necessary to remove an electron from the surface. If an electrical connection is made between two metal surfaces, 1 and 2, then a potential difference $V_1 - V_2$, sometimes called the contact potential difference, arises, given by

$$V_1 - V_2 = \frac{1}{e}(W_2 - W_1) \tag{1}$$

where e is the electronic charge. The work function and hence surface potential may vary over the surface of a polycrystalline material due to regions of different crystal orientation and

[3] We note that after these investigations were carried out, the decision was taken by NASA to descope the ST-7 mission due to cost constraints, and at the time of writing the intention is that the GRS is no longer to be flown as part of the ST-7 mission.

over the surface of an alloy or compound due to nonuniform segregation of the elements [7]. It can also be affected by the presence of contaminants adsorbed on the surface [7–9]. Such differences in surface potential over regions of a surface produce the so-called patch effect. Speake [2] has analysed the effect of such patches to produce forces and force gradients between infinite parallel metallic surfaces in terms of the spatial distribution of the surface potentials. In his analysis, he assumes that the surface potentials are generated by a dipole layer of varying magnitude across the surface. He calculates correlation functions relating the potential distributions across the two facing surfaces. He then calculates the potential energy stored in the electric field between the conductors. The relevant forces and force gradients are found by differentiation with respect to the appropriate directions. By making some assumptions about possible forms for the potential distribution, considered as varying in one dimension, he finds that the force gradients are all of the form

$$\frac{K\varepsilon_0 A v^2}{d^3} \tag{2}$$

where A is the area of each face, ε_0 is the permittivity of free space, v is the standard deviation of the potential fluctuations on the appropriate spatial scale, d is the gap, and K is a dimensionless constant of order 1 related to the assumed form of the power spectrum of the voltage distribution. The appropriate spatial scale in his analysis is that for which the force gradient peaks. For two hypothetical potential distributions he finds that the peak occurs at the values given by $kd \sim 3$ to 5, where k is the spatial frequency of the fluctuations, and K ranges from 1.2 to 1.8. It is noted that gradients in directions perpendicular *and* parallel to the surfaces, giving axial and shear stiffness terms respectively, will contribute to the overall stiffness when applied to the LISA or ST-7 cubic test mass.

In a second paper [10] Speake and Trenkel consider analysis of such forces due to two-dimensional distributions. Extending their analysis to force gradients, we find that for a two-dimensional distribution cylindrically symmetric in k-space, the axial force gradient maximizes at spatial frequencies $kd \sim 2$. The form of the gradient is again similar to that in equation (2), where the value of K depends on the nature of the spatial distribution. For example, if we consider an annular distribution whose Fourier components extend over a decade in spatial frequency centred on the k value given by $kd \sim 2$, we obtain a value of K of $\sim$0.5.

We will extend these analyses to ST-7 and LISA requirements in section 4.

3. Operation of the Kelvin probe and details of the samples studied

The Kelvin probe is a non-contact, non-destructive vibrating capacitor device which measures contact potential difference (V_c) between a conducting specimen and a vibrating probe tip. The particular probe at GSFC used for these measurements is a custom-built UHV system with scanning capability (see figure 1). A general description of the probe operation can be found in [6] and more details in its operating manual [11]. We give a brief description here. A backing potential V_b electrically connects the specimen and probe tip. When $V_b = -V_c$, the circuit is balanced. By using a null measurement technique, the value of V_c can be found accurately. In practice the value of V_c is found by recording the output signal as a function of V_b and fitting the data to find the value of V_b where the signal passes through zero. For all the measurements presented here, the same operating procedure was followed, and the set-up parameters were automatically recorded with each data set. To take a spatial scan, the probe was positioned over the sample to be studied making use of X and Y translators. Once in

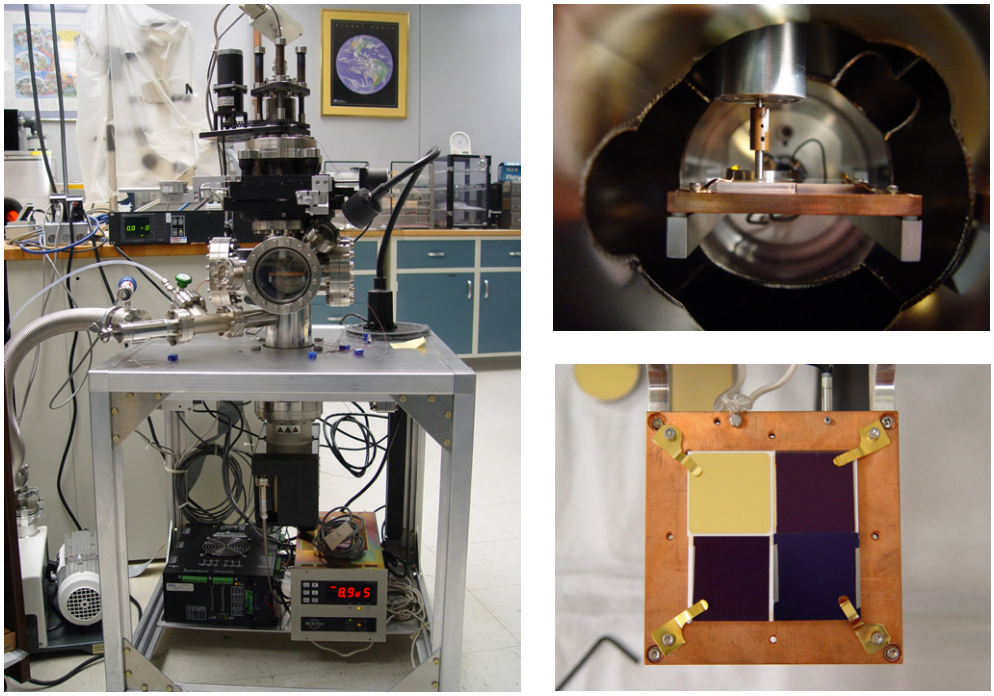

Figure 1. The Kelvin probe at GSFC is shown on the left. A view of the stainless steel probe (diameter 3 mm) positioned above the samples is shown upper right. An example of samples ready for measurements is shown lower right. The samples are (clockwise from upper left): AuNb on alumina, DLC on beryllia, DLCTiAuTi on titanium, DLC on alumina. More details of these coatings, including explanation of the abbreviations, are given in table 1.

position, the probe was lowered in stages, with increasingly fine steps. Its final position is typically approximately 100 μm from the surface.

Table 1 presents a summary of the samples studied to date including details of the substrates and coatings. The majority of the samples were coated in-house at Stanford. All samples were thoroughly cleaned before being shipped to Goddard. The samples were typically 1 inch by 1 inch by $\frac{1}{4}$ inch in size. This size was chosen since it was convenient for coating tests, allowing fabrication of several samples in each coating run. It also fitted with our interest in investigating spatial scales of the order of the gap size (2 mm) or less. The samples were studied in batches of four which was a convenient number to fit onto the sample stage, as shown in figure 1.

One sample has been remeasured during every major run as a witness sample. This was the AuNb coating on an alumina substrate. This one was chosen, rather than for example the AuNb on Au/Pt substrate which would be the default for the test mass materials, due to the fact that the thickness of the Au/Pt sample was different from all the other samples, and for practical reasons it was easier to study four samples of approximately the same thickness. In addition there was one coating which was put into the probe during the first run which could not be studied. This was a diamond-like carbon (DLC) coating on alumina which was insulating rather than conducting, and such coatings cannot be studied in the present configuration of the probe.

The samples chosen for study reflect the various possible materials for the test mass and housing walls and their coatings to be used in ST-7. The test mass will be made of an alloy of

Table 1. Details of all the samples studied including dates. All abbreviations are standard nomenclature for elements, except DLC (diamond-like carbon), DLCc (conducting diamond-like carbon) and ITO (indium tin oxide).

Sample name	Substrate type and coatings listed from substrate surface to outer surface	Measurement date
AuNb on Au/Pt	70% Au 30% Pt alloy substrate (% by atomic weight) + 40 nm Nb + 400 nm Au	Feb 2004
AuNb on alumina	Alumina substrate + 40 nm Nb + 400 nm Au	All runs
DLCc AuNb on Ti	Ti substrate + 40 nm Nb + 400 nm Au + 53.6 nm DLCc	Feb 2004
DLC on BeO	BeO substrate + 40 nm Nb + 200 nm Au + 40 nm Ti + 50 nm DLC	April 2004
DLC AuTiAu on Ti	Ti substrate + 40 nm Ti + 200 nm Au + 40 nm Ti + 50 nm DLC	April 2004
DLC on alumina	Alumina substrate + 40 nm Ti + 200 nm Au + 40 nm Ti + 50 nm DLC	April 2004
AuNb on BeO, closed vias	BeO substrate with 0.64 mm diam vias (2 per substrate), plugged holes filled with thick film gold paste. Both sides of substrate sputter coated with 1 μm Au over Nb	July, August, and Dec 2004
AuNb on BeO, open vias	BeO substrate with 0.64 mm diam vias (2 per substrate)—open holes lined with thick film gold paste. Both sides of substrate sputter coated with 1 μm Au over Nb	July, August 2004
l u AuNb on alumina	Alumina substrate with 400 nm Au over Nb on one side and 1 μm Au over Nb on the other	July, August 2004
TiC on alumina	Alumina substrate + Ti + Cu + Ti + Cu + Ti + TiC (200 nm)	Nov 2004
DLC on Ti	Ti substrate + DLCc (48 nm)	Nov 2004
TiC on Ti	Ti substrate + Ti + Cu + TiC (200 nm)	Nov 2004
AuITO on alumina	Alumina substrate + Au + ITO	Jan 2005
ITO on Ti	Ti substrate + Au + ITO	Dec 2004
AuTiC on alumina	Alumina substrate + Au + TiC (All samples 1 inch by 1 inch by 0.1 inch except Au–Nb on Au/Pt (1 inch diam $\times$ 0.25 inch))	Jan 2005

Au and Pt. The housing walls are baselined to be made of beryllia, with alumina as a fallback. Titanium will be used for inserts in the housing walls. The default coating is Au for the test mass. To avoid problems with sticking of the plunger heads used to cage the mass for launch (which, when retracted, form part of the housing walls), we have been investigating various other coatings for the housing walls. These include DLC, ITO (indium tin oxide) and TiC (titanium carbide), with various underlying layers chosen from adhesion, conductivity and smoothness considerations. One further type of sample studied was a beryllia substrate coated with Au and with vias (holes) through it which would be used for carrying signals through the substrate.

4. Data and results

Two types of data were taken, namely spatial and temporal. Most of the analysis has been done on the spatial scans, and we discuss this first.

4.1. Spatial scans

For these scans, a raster of points was taken, moving 20 steps of 0.5 mm per step in x, holding y constant, then moving 0.5 mm in y and stepping back along the x-direction for 20 steps. The whole raster therefore took data at 400 points and covered a 10 mm by 10 mm square area. The probe tip used throughout had a 3 mm diameter. At each position the contact potential difference between the probe and the sample was measured 11 times, averaged and recorded. It took approximately 1 h to complete one scan.

In table 2 we list all the samples studied with spatial scans (column 1) and the dates of those scans (column 2). In most cases there are two sets of data for each sample. These were generally taken on different areas of the sample, so that we covered a total area which was a significant fraction of the whole surface. To avoid edge effects, we did not scan close to

Table 2. Summary of spatial scans.

Sample name	Date (m/d/yr)	CPD peak to peak and range (mV)	Standard deviation σ_p (mV)	Standard deviation reduced set (mV)
Data taken in February 2004				
AuNb on Au/Pt	2-17-04	33 (−59 to −92)		
AuNb on Au/Pt	2-17(1)-04	16 (−46 to −62)		
AuNb on Au/Pt	2-23-04	38 (30 to 68)	7.4	
AuNb on Au/Pt	2-23(1)-04	26 (39 to 65)		
AuNb on alumina	2-17-04	8 (48 to 56)		
AuNb on alumina	2-25-04	10 (−10 to −20)	1.8	
AuNb on alumina	2-26-04	19 (−16 to −35)		
DLCc AuNb on Ti	2-17-04	134 (−146 to −280)		
DLCc AuNb on Ti	2-26-04	65 (−23 to 42)		
DLCc AuNb on Ti	2-26(1)-04	91 (23 to −68)	19.8	
Data taken in April 2004				
AuNb on alumina	4-7-04	14 (117 to 131)		
DLC on BeO	4-9-04	17 (367 to 384)		
DLC on BeO	4-14-04	22 (483 to 505)	4.4	4.4, 5.0
DLC AuTiAu on Ti	4-14-04	20 (507 to 527)	4.2	
DLC AuTiAu on Ti	4-15-04	16 (480 to 496)		
DLC on alumina	4-15-04	17 (270-287)	3.7	
DLC on alumina	4-15(1)-04	19 (299 to 318)		
Data taken in July (faulty ion pump) and August 2004				
AuNb on alumina	7-19-04	59 (291 to 350)		
AuNb on alumina	8-10-04	13 (151 to 164)	3.3	
AuNb on alumina	8-13-04	18 (144 to 162)		
Au on BeO, closed vias				
Not near via	7-19-04	72 (139 to 211)		
?	7-19-04(1)	64 (128 to 192)		
Not near via	8-11-04	57 (83 to 140)	11.3	9.1, 9.6
Not near via	8-11-04(1)	20 (88 to 108)		
Over closed via	8-12-04	52 (86 to 138)		
Au on BeO, open vias				
Not near via	7-20-04	59 (80 to 139)		
Over open via	7-20-04(1)	68 (69 to 137)		
Over open via	7-20-04(2)	69 (65 to 134)		
Not near via	8-12-04	20 (75 to 95)		
Over open via	8-12-04(1)	40 (60 to 100)	8.2	
Not near via	8-13-04	19 (75 to 94)		
1 u Au on alumina	7-21-04	53 (77 to 130)		
1 u Au on alumina	7-21-04(1)	561 (72 to 633)		
1 u Au on alumina	7-21-04(2)	296 (69 to 365)		
1 u Au on alumina	7-21-04(3)	179 (−52 to +127)		
1 u Au on alumina	8-13-04	25 (76 to 101)	5.1	
1 u Au on alumina	8-13-04(1)	28 (74 to 102)		

Table 2. (Continued.)

Sample name	Date (m/d/yr)	CPD peak to peak and range (mV)	Standard deviation σ_p (mV)	Standard deviation reduced set (mV)
Data taken in November 2004				
AuNb on alumina	11-02-04	12 (−177 to −189)	2.1	
AuNb on alumina	11-03-04	10 (−180 to −190)	1.4	1.0, 1.3
TiC on alumina	11-03-04	6 (−325 to −331)	1.2	
TiC on alumina	11-03-04(1)	6 (−325 to −331)		
DLC on Ti	11-04-04	7 (−292 to −299)	1.5	
DLC on Ti	11-04-04(1)	8 (−291 to −299)		
TiC on Ti	11-04-04	6 (−328 to −334)	1.3	
TiC on Ti	11-05-04	7 (−330 to −337)		
Data taken in early December 2004				
AuNb on alumina	12-07-04	7 (−207 to −214)		
AuNb on alumina	12-08-04	8 (−231 to −239)		
Au on BeO, closed vias				
Not near	12-08-04	18 (−222 to −240)		
Over closed via	12-08-04	14 (−210 to −224)		
Over closed via	12-08-04(1)	16 (−208 to −224)	3.3	
Data taken in late Dec 2004/early Jan 2005				
AuNb on alumina	12-28-04	9 (−204 to −213)		
AulTO on alumina	1-03-05	5 (−229 to −234)	1	
AulTO on alumina	1-03-05(1)	4 (−225 to −229)		
ITO on Ti	12-29-04	5 (−272 to −278)	1.3	
ITO on Ti	12-30-04	9 (−265 to −274)		
AuTiC on alumina	1-04-05	8 (−179 to −187)	1.6	
AuTiC on alumina	1-04-05(1)	5 (−182 to −187)		
Data taken in late Jan 2005				
ITO on Ti	1-21-05	5 (−219 to −214)		
ITO on Ti	1-21-05(1a)	6 (−216 to −222)		
ITO on Ti	1-21-05(1b)	6 (−216 to −222)		

the edges of the samples. In the third column of table 2 the peak-to-peak variation and the range in contact potential difference (CPD) are given. The fourth column gives the standard deviation of the CPD values of the full set of data for a particular scan for a representative subset of scans, and the fifth column records the standard deviation for a reduced set of data points, discussed further in section 4.2.

4.2. Observations from the spatial data

The first observation is that in general data taken in later runs (November 2004 onwards) show a reduced variation in the peak-to-peak value, with that number being around or below 10 mV regardless of type of coating, except for the via samples. The major difference between runs before and after November was the pressure in the chamber. In the early runs this was of order

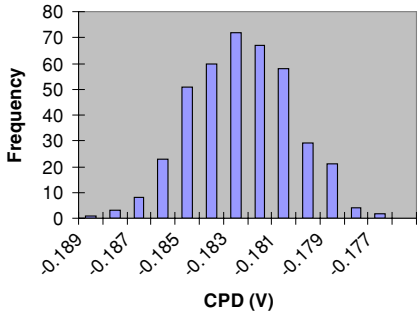

Figure 2. Histogram of CPD values for the AuNb on alumina data taken on 2-11-04. Values range from −0.177 to −0.189 V, corresponding to a peak-to peak value of 12 mV. Standard deviation of the distribution is 2.1 mV.

10^{-7} mbar and from November onwards of order 10^{-9} mbar. The witness sample (AuNb on alumina) has been fairly consistent throughout—with some higher values (19 mV, 14 mV) in early runs, but in general around 10 mV. Among other things to note is that the first DLC coating studied in February was rather noisy (∼100 mV). However it was observed that this DLC coating did not adhere well to its underlying Au layer, and this could be the main factor for the marked difference in behaviour between that DLC coating and others subsequently studied. We also observe that data taken in July were uniformly noisy and this was attributed to the effects of a faulty ion pump.

To use these results to compare with requirements in terms of allowed variation, we need to calculate the standard deviation, σ_p, of the CPD over the surface, where the subscript 'p' is used to denote that this is the standard deviation for a particular probe size. This has been done for a representative set of samples (table 2, column 4), and it can be seen that the standard deviation is around a factor of 5 to 7 less than the peak-to-peak value. We illustrate this finding with an example of a histogram of CPD values for one of the scans of the witness sample; see figure 2. Since the scans are stepped in 0.5 mm steps and the probe size is 3 mm, each value recorded will not be uncorrelated with the next, and this complicates the interpretation of the standard deviation of the whole data set. To get an idea of the significance of this correlation, in a few cases the standard deviation has been calculated for a reduced set of data points which formed an array of every sixth point in the x- and y-directions. This was done for two sets of points in each case, starting from a different initial position in the array. From a simple argument such an array of readings should be essentially uncorrelated. It can be seen that where this calculation has been done (column 5 in table 1) the numbers are not dissimilar to the standard deviation of the full set of data, and so to the precision that we need to be able to draw some conclusions on meeting requirements, we can use the standard deviation of the full set.

An immediate observation that we can make from the data in table 2 is that when the same sample is studied at different times, the absolute value of the CPD can vary widely. For example the AuNb on alumina witness sample has yielded values of CPD from ∼ −140 mV to +350 mV during the various runs where samples have been removed from the vacuum chamber and then replaced. Some of that variation could be due to changes in the electrical contact to the samples. However we also see variation on different days within a single run, i.e. when the samples have remained in place. Such changes could be due to surface changes on the sample, the probe tip or both, and is strongly suggestive of the presence of surface contaminants. An idea of repeatability on shorter timescales, of interest for ST-7 and LISA, can be found from the temporal data, discussed later.

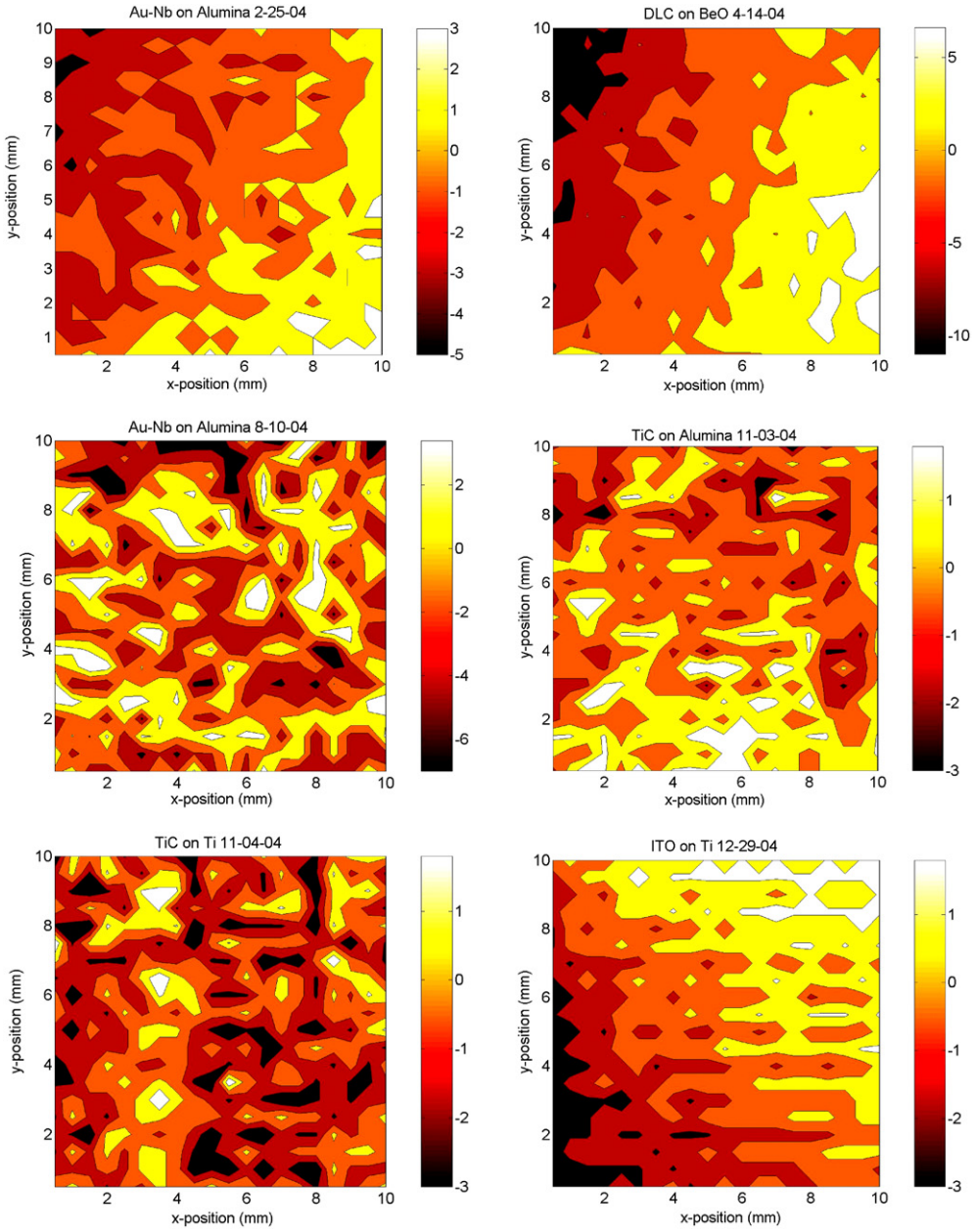

Figure 3. Examples of contour plots of contact potential difference in millivolts over a 10 mm by 10 mm area. The value of offset subtracted/added from each data point is given below. Top left: AuNb on alumina (25-2-04), offset of 15 mV added. Top right: DLC on BeO (14-4-04), offset of 494 mV subtracted. Middle left: AuNb on alumina (10-8-04), offset of 158 mV subtracted. Middle right: TiC on alumina (3-11-04), offset of 328 mV added. Bottom left: TiC on Ti (4-11-04), offset of 331 mV added. Bottom right: ITO on Ti (29-12-04), offset of 275 mV added.

To get an idea of the distribution of the CPD values across a particular sample, we have taken the data and plotted it in contour plots using a MATLAB routine. This has proved useful in revealing certain characteristics of the data. Some examples are shown in figure 3.

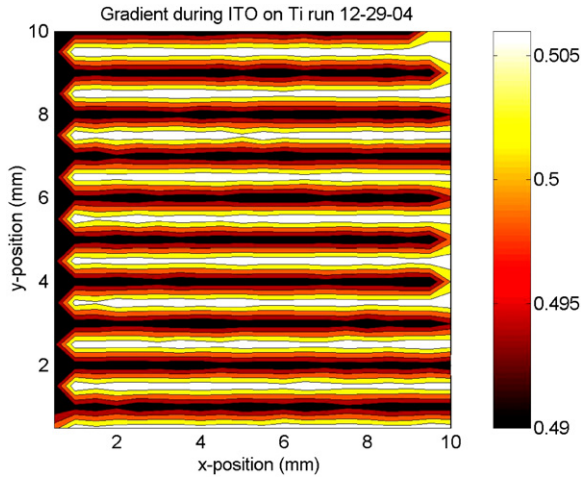

Figure 4. Example of gradient values plotted as a function of position, taken during the scan of ITO on Ti shown in bottom right in figure 3.

It should be noted that we have used four levels of contour for these plots. A larger number of levels was tried but did not reveal significantly more information. In these plots we have also subtracted an offset from the CPD values so that the values are approximately centred about zero in each case.

Firstly we see that in some cases there is an apparent structure to the CPD variations—this can be seen most noticeably in the top two plots and bottom right in figure 3, where there appears to be a general slope in the values, not always in the same direction. In the other figures shown the variations appear more random. We do not know what is causing the apparent structure. However we speculate that this effect could be due to surface contamination which has spread from a particular direction.

It is interesting to note that two of the plots (top left and middle left) are of the same sample (the witness sample), and the first shows structure whereas the second does not. Thus if surface contamination is the cause of the apparent structure, its effect can change with time.

We noted in some of the later runs that there was another type of structure appearing in the data. This can be seen clearly in the bottom-right plot of figure 3, where there is evidence of 'stripiness' in the x-direction. On looking back at the raw data, very marked stripiness of exactly the same form was found in the values of the gradient recorded as each measurement was made. This gradient is the ratio of the output signal to the applied backing potential and as such is a function of the separation of the probe and sample. When in operation a dc offset adjusts to hold the gradient at the chosen value, 0.5 in our case, equivalent to holding the probe–sample distance constant. The stripy effect is seen in all gradient data, and an example is shown in figure 4. We note that the stripes line up with the direction in which the probe is stepped to take data—along the x-direction and then up one step in the y-direction and back in the negative x-direction. The nominal value for the gradient was 0.5. The actual values average around 0.51 for the left to right scans and 0.49 for the right to left scans (where left and right correspond to increasing and decreasing values of x, respectively.)

We contacted the manufacturer about this effect. Firstly they noted that the absolute range of CPD variation we were observing was approaching the limits of the sensitivity of the device. Regarding the particular effect seen, the general conclusion was that mechanical hysteresis was the likely cause. The XY stage is driven by a stepper motor which has some backlash.

This results in the probe height relative to the sample changing depending on the direction of motion, and hence the gradient changes. The dc offset adjusts to correct the gradient change, but only to a precision of ±0.01 in the default gradient value of 0.5. The work around used in atomic force microscopes to reduce a similar hysteresis effect is to take data in one direction only. The manufacturer further commented that trying to remove the effect by post-processing of the data would not be a straightforward procedure.

4.3. Interpretation of data compared to requirements

The ST-7 requirement on rms of the contact potential variation, σ, is a maximum of 100 mV based on the theoretical analysis of Speake [2]. This value comes from a requirement on the total stiffness per unit mass (or force gradient) due to the patch effect to be less than 10^{-7} s^{-2}. Schumaker in [3] also uses 100 mV as the working assumption in her noise budget analysis for LISA. To compare our results to this requirement, we need to extrapolate our results taken using a probe diameter of 3 mm to the relevant spatial frequency. We present three different ways to carry out this extrapolation.

In the first instance, we assume that the power spectrum of fluctuations is flat up to some maximum value of spatial frequency k_m. From Speake's analysis for such a distribution (in one dimension), the maximum force gradient occurs at a spatial frequency given by $k_m d \sim 5$ where d is the gap size between test mass and housing, corresponding to an inverse spatial frequency of 0.4 mm for a gap size of 2 mm. We have observations of the fluctuations σ_p^2 at a frequency of 1/(probe diameter), denoted by k_p. We can thus deduce the power fluctuation σ^2 at a spatial frequency of k_m by assuming a flat distribution and using the relationship

$$\frac{\sigma^2}{k_m} = \frac{\sigma_p^2}{k_p}. \tag{3}$$

With $k_m = (0.4\ \text{mm})^{-1}$ and $k_p = (3\ \text{mm})^{-1}$, we deduce that $\sigma = (3/0.4)^{1/2}\,\sigma_p = 2.7\sigma_p$.

To satisfy the requirement of 100 mV, we require σ_p to be less than ~37 mV. Typical values for the standard deviation σ_p are 1 to 4 mV, and even for the relatively noisy via samples the number is around 10 mV. Thus it would appear that all the samples studied, apart from the earliest DLC sample, meet the requirements.

An alternative distribution which can be considered is that all the patches are of similar size, characteristic of the typical size of the surface crystallites of the material; see for example Camp *et al* [7]. Within a probe area there will be N such patches where N is the area of the probe divided by the typical area of a patch. From a statistical argument, if the rms variation in surface potential measured with a probe area A_p is σ_p then the rms variation on any smaller area A (equal to or larger than the intrinsic patch size) will be $\sqrt{N}$ larger where $N = A_p/A$. We can use this argument to find the fluctuations on any areal size that is relevant to our analysis. For example if the sizes of patches which maximize the force gradient for this type of distribution are also approximately those with linear dimensions of $d/5 = 0.4$ mm then we can deduce that the rms fluctuations σ on this scale will be given by

$$\sigma = \sqrt{N}\sigma_p = (3/0.4)\sigma_p = 7.5\sigma_p. \tag{4}$$

Thus using this argument we find that if σ has to be 100 mV or less, σ_p should be 13 mV or less. Again all the samples studied, apart from the earliest DLC sample, meet this requirement, which is more severe than that from the first analysis considered above.

If finally we consider the particular two-dimensional distribution discussed at the end of section 2, the maximum force gradient occurs at a spatial frequency given by $k_m d \sim 2$.

Thus patches of linear size $d/2 = 1$ mm are most important. Applying the above statistical argument, we would find that $\sigma = \sqrt{N}\sigma_p = (3/1)\sigma_p = 3\sigma_p$. For σ to be 100 mV or less we require σ_p to be 33 mV or less, which is satisfied by our measurements.

We have presented three different analyses here. We do not know which assumption on distribution of patches is closer to the actual distributions in our measurements—a flat spectrum of fluctuations, a fixed size of patches or some other distribution. Clearly we have also found that the spatial maps are not always random in appearance and this must affect our interpretation in those cases. In particular, to be more confident in our interpretation of the results compared to requirements, we need information on smaller scales, closer to that at which the force gradients maximize.

It is appropriate here to comment on the accuracy of the data we have been using. A *single* CPD measurement has an accuracy of ~2.5 mV, limited by the 12 bit A/D converter used in the data recording system. In carrying out the measurements we averaged 11 readings for each data point, thus reducing the random variation by approximately a factor of 3. The data are then recorded to 1 mV. This level can be taken as the accuracy of each recorded data point. Our more recent measurements, where peak-to-peak values were typically ~6 mV, are thus coming close to the current limit. We return to this point in the discussion on temporal variations.

4.4. Temporal data

For these measurements the probe tip remained at the same place and measurements, on a few second time intervals, were taken for several thousand seconds typically. Two scans were typically done per sample per run at different positions. The duration was chosen to investigate changes of relevance to the operating frequency of ST-7 (1 to 30 mHz).

Typically the variation was a few mV for earlier runs, reducing to sub mV for the later runs at lower pressure (November onwards), with one or two exceptions. We deduce that the lower pressure has in general decreased the variation. In figure 5 we show two examples each from two samples, from an early and later run. It can be seen that the variation is much smaller in the later run. These traces have been plotted using a package called MINITAB with a LOWESS (locally-weighted scatter plot smoother) routine [12] which gives a smoothed curve by averaging. This routine calculates a new smoothed y-value for each (x, y) point by taking a chosen fraction (the default value of 0.5 in our case) of all the points centred about the particular x value of interest and performing a weighted linear regression on that set of points. It is instructive to see what the raw data look like and this is also shown in figure 5 corresponding to that of one of the early time sets shown. The quantization in mV steps can clearly be seen.

4.5. Interpretation of temporal results compared to possible noise source in LISA

In [3] Schumaker considers the magnitude of the noise associated with temporal fluctuations in CPD and its effect in LISA. She uses a figure of 10^{-5} V Hz$^{-1/2}$ at 10^{-4} Hz in her noise budget, and comments that a value ten times larger, in combination with a dc offset of 30 mV or net free charge of 10^{-13} C on the test mass, could produce a disturbance which would dominate the total acceleration noise budget, assuming that the gap size remains at 2 mm. Thus we need to be able to measure the CPD fluctuations at levels of sub mV Hz$^{-1/2}$ for LISA, at frequencies down to 10^{-4} Hz. An example of a fast Fourier transform of some temporal data is shown in figure 5, using the data from one of the later runs when the temporal variations were

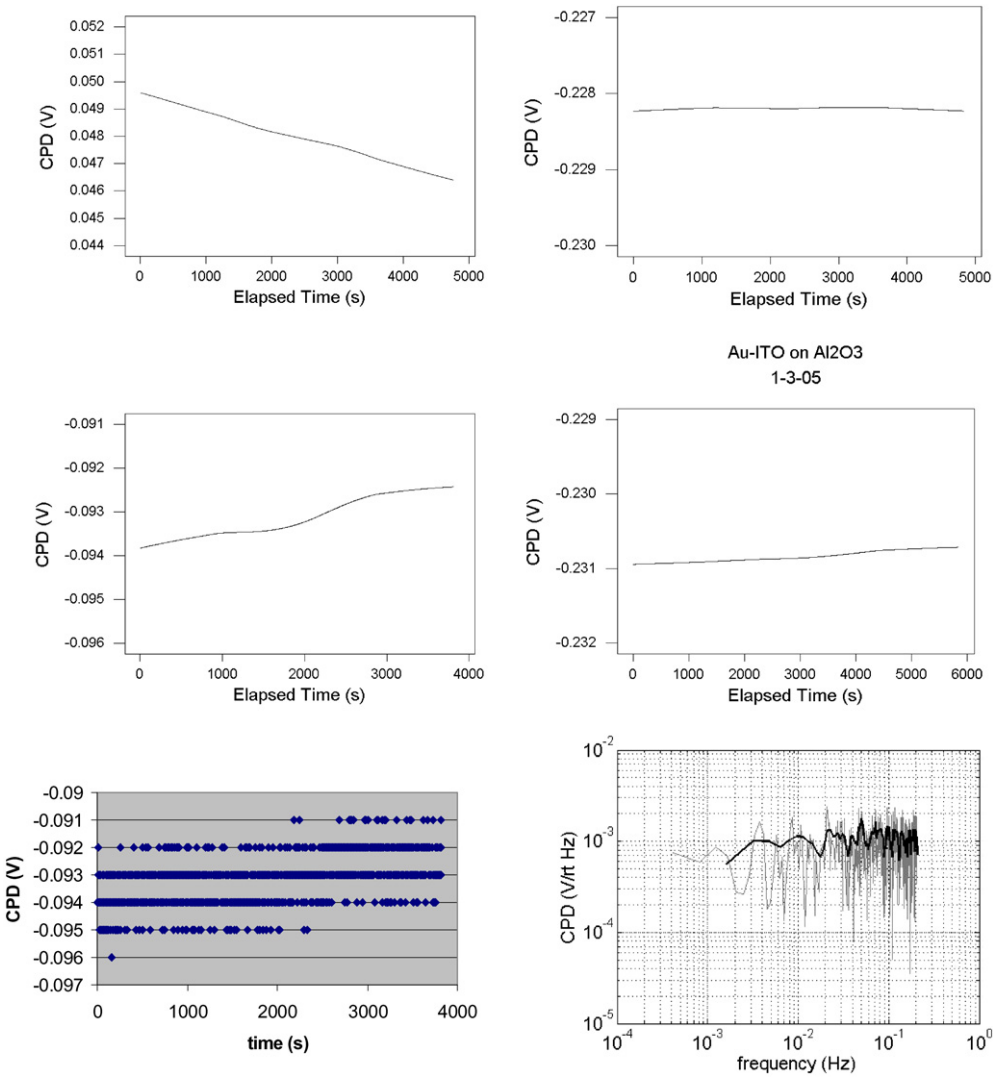

Figure 5. Time variations of contact potential differences. Top and middle left: Au on Au/Pt, data taken on 23-2-04 and 17-2-04 respectively, smoothed using a LOWESS routine. Bottom left: raw data for the plot shown middle left. Top and middle right: Au/ITO on alumina, both sets of data taken on 03-1-05, smoothed using a LOWESS routine. Bottom right: amplitude spectral density of the first 2400 s of raw data for plot on middle right, grey line—unaveraged, black line—with averaging.

smaller. The first 1000 points (corresponding to 2400 s) were used in the analysis, which for the current implementation of the recording software is the longest stretch of data over which the time intervals are equal. It can be seen that the amplitude spectral density shows a value of approximately 1 mV $Hz^{-1/2}$ over a range from $\sim 4 \times 10^{-4}$ Hz to 0.2 Hz with no obvious spectral features. This result is almost certainly limited by the accuracy of the data. Thus with the present sensitivity limited at $\sim$1 mV we are not as yet able to carry out investigations at the noise levels for LISA considered in [3].

5. Conclusions and future work

Our results and analyses to date suggest that any of the materials studied appear to meet the spatial requirements for ST-7 and LISA. However we have had to make several assumptions in arriving at that conclusion, as described in section 4.3. More work is needed to see if these assumptions are valid. The data also revealed evidence of behavioural trends with pressure and possible contamination effects, both of which require further study. For temporal variations, we noted that in general the variation decreased with decreasing pressure, with changes of a few mV in several thousand seconds typical for earlier runs when the pressure was of order 10^{-7} mbar, typically reducing to sub mV for the later runs at a pressure of order 10^{-9} mbar. We also noted that the accuracy of the instrument at present is not sensitive enough to allow spectral density investigations at the noise levels required for LISA.

5.1. Spatial studies

The mechanical hysteresis which is believed to be the cause of the line-like structure seen in recent spatial results needs to be further investigated. The manufacturer has given us several ideas to pursue to reduce this effect of which the simplest would be to carry out scans in one direction only.

5.1.1. Use of smaller probe tip size. To compare our results to theory, we ideally need information on CPD variations as a function of spatial frequency. We have made some assumptions to interpret the 3 mm results, but we cannot be sure which assumptions are valid without taking smaller scale measurements. We note that at present the probe size is larger than the expected gap size of 2 mm in LISA, whereas patch variability somewhat smaller than the gap size is likely to be most important. A 1 mm probe tip is available for use. However it is noted that signal-to-noise decreases with the probe area, which may limit what can be done with a smaller probe.

5.1.2. Investigation of pressure effects. It is important to establish if the variation in magnitude of patch effect with pressure is a real effect. This is particularly of interest since the working pressure around the test mass in ST-7 (and possibly LISA) is specified to be $\sim 10^{-7}$ mbar, at which the spatial fluctuations appear to be larger. A systematic study of CPD as a function of pressure should be carried out.

5.1.3. Investigation of contaminants. There is a strong indication that contaminants are affecting the results. For example, the structure of the CPD variations for the witness sample appears to be different during different runs. It has been reported [9] that contaminants generally produce patches over length scales larger than the crystallite size, and can, given sufficient time, smooth out potential variations. Our results are consistent with surface contamination causing the large scale structure discussed in section 4.2. In another previous study of CPD variations [7] evidence was found that surface reactions with contaminants promoted surface potential structure on various conducting materials, with gold and graphite being the least affected of the materials investigated. There are several potential sources of contamination in ST-7 and LISA: e.g. water, epoxies used to stake screws and wire insulation material. While materials with low outgassing qualities are specified, the impact of even a monolayer of contaminant on the test mass or electrode surfaces could be significant. A controlled investigation using known release of contaminants could be carried out, and a port on the Kelvin probe vacuum system is available for introducing contaminants. In addition,

ultraviolet light is used to control the test mass charge by shining it on the very surfaces that are sensitive to surface contamination. The impact of the ultraviolet light on the presence of surface contaminants should be investigated as well.

5.1.4. Investigation of temperature effects. There is provision for including a thermocouple within the copper block on which the samples sit. Its use would allow correlations between temporal changes in potential difference and temperature to be investigated.

5.2. Temporal investigations

An increase in the accuracy of measurement (to significantly better than 1 mV) is needed to investigate temporal variations of patch effects for LISA, where the requirement is likely to be 10^{-4} V Hz$^{-1/2}$ or less for the current gap size. An upgrade to the A/D electronics is required to reduce the noise level to $\sim$10 μV Hz$^{-1/2}$ and this upgrade is under investigation with the manufacturer. Software to allow recording at evenly-spaced time intervals for at least 10 000 s would also be advantageous for the Fourier analysis.

5.3. General comments

The effects of spatial and temporal fluctuations in patches can also be studied by directly measuring the forces produced using a sensitive torsional pendulum such as has been developed at the University of Trento [13, 14]. This group has recently reported [14] that an observed residual stiffness could be explained by patch voltages of the order of 100 $\mathrm{mV_{rms}}$ homogeneously distributed across the sensor housing. Clearly further investigations of these phenomena are important for LISA, including comparison of results using different measurement techniques. Finally we note that the ST-7 and LISA requirements given in this paper assume a gap size of 2 mm between the test mass and its housing. Spatial patch effects decrease with the gap size as $1/d^3$ and temporal effects decrease as $1/d^2$. If the gap size were increased, these effects would rapidly decrease to the extent that they might no longer be considered significant noise sources for LISA.

Acknowledgments

We would like to thank Henry Abakians, Bob McAllister, Alex Romanovsky and Clive Speake as well as colleagues at Stanford University for help on this project. The work at Stanford University was partially supported under JPL contract 1232133 as part of the ST-7 drag reduction system (DRS) and partially supported under JPL contract 1258294 (LISA Gravitational Reference Sensor Technology Development Plan).

References

[1] LISA Study Team (Bender P *et al*) 1998 *LISA: Laser Interferometer Space Antenna for the Detection and Observation of Gravitational Waves: Pre-Phase A Report MPQ 233* 2nd edn (July 1998) (Garching, Germany: Max Planck Institut für Quantenoptik)

[2] Speake C C 1996 *Class. Quantum Grav.* **13** A291–7

[3] Schumaker B L 2003 *Class. Quantum Grav.* **20** S239–53

[4] Stebbins R T, Bender P L, Hanson J, Hoyle C D, Schumaker B L and Vitale S 2004 *Class. Quantum Grav.* **21** S653–60

[5] Hanson J, Keiser G, Buchman S, Byer R L, Lauben D, Shelef B, Shelef G, Hruby V and Ganero-Castano M 2003 Disturbance reduction system: testing technology for drag-free operation *Gravitational Wave*

Detection: Proc. SPIE Conf. on Astronomical Telescopes and Instrumentation vol 4856, ed M Cruise and P Saulson (Bellingham, WA: SPIE Optical Engineering Press) pp 9–18

[6] http://www.mcallister.com/kppage1.html

[7] Camp J, Darling T W and Brown R E 1992 *J. Appl. Phys.* **71** 783–5

[8] Camp J, Darling T W and Brown R E 1991 *J. Appl. Phys.* **69** 7126–9

[9] Rossi F and Opat G I 1992 *J. Phys. D: Appl. Phys.* **25** 1349–53

[10] Speake C C and Trenkel C 2003 *Phys. Rev. Lett.* **90** 160403

[11] http://www.mcallister.com/kpdnload.html

[12] MINITAB Statistical Software 1999 *User's Guide 1: Data, Graphics, and Macros* Release 13. (Minitab, Inc.) http://www.minitab.com

[13] Carbone L, Cavalleri A, Dolesi R, Hoyle C D, Hueller M, Vitale S and Weber W 2003 *Phys. Rev. Lett.* **91** 151101

[14] Carbone L, Cavalleri A, Dolesi R, Hoyle C D, Hueller M, Vitale S and Weber W J 2005 *Class. Quantum Grav.* **22** S509–19